S. Niksa, G.-S. Liu, L. G. Felix, P. V. Bush, and D. M. Boylan, "Predicting NO_X Emissions from Biomass Cofiring," 28th Int. Technical Conf. on Coal Utilization and Fuel Systems, Coal Technology Assoc., Clearwater, Fl, March, 2003.

PREDICTING NO_X EMISSIONS FROM BIOMASS COFIRING

Stephen Niksa[a], Guisu Liu[a], Larry Felix[b], P. Vann Bush[b], and Douglas M. Boylan[c]

[a]Niksa Energy Associates, 1745 Terrace Drive, Belmont, CA 94002, neasteve@pacbell.net
[b]Southern Research Institute, P. O. Box 55305, Birmingham, AL, 35255-5305
[c]Southern Company Services, Inc., P. O. Box 2641, Birmingham, AL, 35291-8195

ABSTRACT

This research features an extensive database of NO_X emissions from 1.7 MW_t pilot-scale flames of two biomass forms on four coals, and quantitative interpretations based on the most extensive chemical reaction mechanisms available. Each biomass/coal combination was evaluated at furnace stoichiometries that generated exhaust O_2 levels from 2.5 to 5.0 %, in an unstaged flame and a staged flame with 15 % overfire air. Flames with at least two biomass loadings were compared to a coal-only flame in every case.

Under simulated tangential-firing, cofiring with sawdust and switchgrass significantly reduced NO_X emissions, provided that the biomass was co-milled with the coal and co-injected into the flame. Even in cases where the biomass contained more fuel-N than the reference coal, cofiring significantly reduced NO_X emissions. The magnitude of the NO_X reduction generally increased in proportion to the biomass loading, although several cases with switchgrass exhibited greater extents of NO_X reduction at 10 % loading versus 20 %. Our analysis predicts the favorable impact of biomass cofiring within useful quantitative tolerances across the full range of fuel quality in the test program. The fuels' proximate and ultimate analyses were used to predict the compositions of all volatile and residual fuel compounds, which were then processed through full chemistry in the gas phase and on soot to describe fuel-N conversion. Biomass cofiring yields lower NO_X levels because biomass generates more gaseous volatiles and less soot, which promotes NO reduction; and it also expels less char-N into downstream flame zones.

INTRODUCTION

In theory, biomass cofiring should reduce NO_X emissions simply because most biomass forms contain less fuel-N than the coals they displace. The yields of volatiles are generally much higher from biomass than from coal, and volatiles contain many compounds that can effectively reduce NO in fuel-rich flame zones. Biomass also decomposes faster than coal, which tends to steepen near-burner temperature profiles and enhance the ignition characteristics. These factors are expected to improve NO_X emissions by more than the displacement of coal-N. But the database from pilot- and full-scale testing exhibits mixed results, including substantial representation for no effect, for less reduction than the displacement of fuel-N, and for enhanced reduction over the displacement of fuel-N.

The premise for our work is that uncontrolled variables are responsible for the ambiguities in the existing database. A testing campaign was staged to characterize the most likely parameters, including the biomass form, coal type, biomass injection configuration, burner staging, and furnace stoichiometry. The database from the testing campaign was then interpreted with simulations based on full chemistry for fuel

decomposition, volatiles combustion including fuel-N conversion, soot conversion, and char burnout. Once the model predictions were demonstrated to be accurate, the simulation results were interrogated to determine how the biomass affected NO_X emissions. We find that two factors determine whether biomass cofiring will reduce NO_X emissions: (1) Does the abundance of gaseous volatiles, not soot, from biomass reduce away the NO formed near the burner; and, (2) Is significantly less char-N released into downstream flame zones by the addition of biomass. This paper emphasizes the interpretation of the database with detailed chemical reaction mechanisms. More thorough descriptions of the simulation methodology are available (Niksa and Liu, 2002a and 2003).

TESTING PROGRAM

All tests were conducted in Southern Research Institute's (SoRI) Combustion Research Facility (CRF). The CRF consists of fuel handling and feeding systems, a vertical refractory lined furnace with a single up-fired burner, a horizontal convective pass, heat exchangers and conventional exhaust cleaning devices. Emissions from this system have been qualified against those from full-scale, tangential-fired furnaces for the operating conditions imposed in this work (Monroe et al., 1995). The 8.5 m by 1.07 m (i.d.) cylindrical furnace handles gas velocities from 3 to 6 m/s, and residence times from 1.3 to 2.5 s. The nominal firing rate is 1.7 MW_t, which was fixed for all cases in this work. A single burner generates a core of pulverized fuel and primary air surrounded by weakly swirled secondary air. For all cases in this paper, the biomass was co-milled with the coal and the mixture was directly fed into the burner. Overfire air (OFA) was injected through 4 off-radius ports located 4.6 m down the furnace. All datasets include cases with 0 (unstaged) and 15 % OFA. In the unstaged series, the OFA was combined with secondary air. Air feedrates were varied to produce exhaust (wet) O_2 levels between 2.5 and 5 %.

Fuel quality was varied by firing four diverse coals with two forms of biomass. Properties of the six primary fuels appear in Table 1 in order of increasing rank from left to right. Moisture levels are highest for the low-rank fuels, especially SG and JR. Ash levels are widely variable and high for biomass SG and for coals PR and JW. Whereas it appears that the volatility of SD is much higher than SG's, on a dry-ash-free (daf) basis, their volatiles are almost identical. The daf-volatiles contents of the coals fall by more than a factor of two over this suite of samples, which will definitely affect the conversion of coal-N into NO_X. Carbon contents increase and oxygen contents decrease for fuels of progressively higher rank. The pair of biomass samples represents most of the range of elemental compositions seen for diverse forms of biomass. The represented range of coal rank, from subbituminous through lv bituminous, is similarly broad. The hydrogen, nitrogen, and sulfur levels are not rank-dependent. Whereas almost all biomass contains little nitrogen and sulfur, sample SG contained the most nitrogen of any of the fuels, due to its decomposition before firing. The particle size distributions (PSDs) are typical utility grinds for the coals, except for the much finer grind of JR, whereas the biomass grinds are much coarser, as expected. The pairs of Rosin-Rammler parameters were assigned from pairs of size fractions provided by SoRI.

COMPUTER SIMULATIONS

It is not currently possible to incorporate detailed chemical reaction mechanisms into conventional CFD simulations of pulverized fuel (p. f.) flames. Since chemistry in the gas phase, especially volatile-N conversion chemistry, was suspected to play a dominant role in NO_X production during biomass cofiring, Niksa Energy Associates developed a new computational approach for this application based on our "Advanced Post-Processing (APP)" method. The APP method first generates an equivalent network of idealized reactor elements from a conventional CFD simulation. The reactor network is a computational environment that accommodates realistic chemical reaction mechanisms; indeed, mechanisms with a few thousand elementary chemical reactions can now be simulated on ordinary personal computers, provided that the flow structures are restricted to the limiting cases of plug flow or perfectly stirred tanks. The network is "equivalent" to the CFD flowfield in so far as it represents the bulk flow patterns in the flow.

Table 1. Fuel Properties.

	Sawdust **SD**	Switch Grass **SG**	Jacobs Ranch **JR**	Galatia **GL**	Pratt **PR**	Jim Walters **JW**
Proximate, as rec'd						
Moisture	9.5	15.2	19.3	5.8	1.9	0.8
Ash	0.4	29.5	5.4	6.6	15.1	14.6
Volatile Matter	78.1	47.6	39.6	33.7	33.2	20.0
Fixed Carbon	11.9	7.7	35.7	54.0	49.9	64.6
Ultimate, daf wt. %						
C	49.8	56.1	74.9	81.8	83.4	89.5
H	6.1	5.4	4.9	5.0	5.5	4.6
O	43.9	35.7	18.8	10.0	7.5	3.3
N	0.2	2.4	0.9	2.0	1.8	1.7
S	0.0	0.4	0.4	1.1	1.8	0.9
PSD						
$<d_P>$, μm	163	173	29	53	48	34
RR-n	2.1808	2.2617	0.9405	1.7353	1.3111	1.0082
RR-b, cm	5518.2	6728.2	169.71	6116.5	752.06	211.46

Such equivalence is actually implemented in terms of the following operating conditions: The residence time distributions (RTDs) in the major flow structures are the same in the CFD flowfield and in the section of the reactor network that represents the flow region under consideration. Mean gas temperature histories and the effective ambient temperature for radiant heat transfer are also the same. The entrainment rates of surrounding fluid into a particular flow region are evaluated directly from the CFD simulation. To the extent that the RTD, thermal history, and entrainment rates are similar in the CFD flowfield and reactor network, the chemical kinetics evaluated in the network represents the chemistry in the CFD flowfield. Whereas this paper emphasizes the application to biomass cofiring, separate publications explain the simulation methodology in greater detail (Niksa and Liu, 2002a and b; 2003).

CFD Simulations

CFD simulations of the CRF were performed by Reaction Engineering International (REI) for tests with PR coal and various biomass. Cases with JR and JW were performed at SoRI, using REI's Configurable Fireside Simulator (CFS) for the CRF. The CFS imposes a fixed computational grid on the calculations, and enables parametric case studies with the same firing configurations. No CFD were available for cases with GL coal because these flame structures were expected to be very similar to the PR flames.

The most surprising feature in the CFD simulations is that all fuel particles remained on the furnace axis throughout this furnace. Neither mixing in the near-burner zone nor radial OFA injection disperses the particles off their original trajectories. Near the burner, the primary air stream was significantly expanded by the release of volatiles from the fuel suspension and by thermal expansion. This expansion zone delineates a fuel-rich core from the outer, annular flow of secondary air. Nominal residence times in the core range from 120 to 170 ms. The expansion of the primary flow promotes entrainment of secondary air into the core, because some of the secondary flow penetrates the expansion boundary. In addition, a portion of secondary air is entrained into the core as soon as it passes the edge of its delivery tube in the

fuel injector. Together, these entrainment mechanisms almost instantaneously mix about 20 % of the secondary air into the primary flow.

The mixing layer between the core and secondary air streams gradually expands until it contacts the furnace wall midway to the OFA ports. An external recirculation zone (ERZ) forms in the corner bounded by the outer boundary of the secondary air stream, but is too weak to entrain particles or appreciable amounts of air or fuel compounds. As the fuel compounds in the flame core contact the secondary air stream, they mix and burn in an expanding mixing layer. This layer completely surrounds the core near the burner inlet, and fills the entire furnace downstream of the core. The most distinctive feature of the mixing layer is that the temperature profile across the layer in the normal direction passes through a maximum value which is essentially the same around the entire circumference of the core. Maximum gas temperatures approach 1700°C in cases where fuels of the highest heating values were fired without OFA, and 1600°C in cases with 15 % OFA. Residence times in the mixing layer to the OFA location vary from 500 to 600 ms. The four air jets from the OFA ports do not penetrate onto the centerline. They also do not fill the entire flow cross section. Downstream of the OFA ports, the flow relaxes to a plug flow pattern that carries ash and exhaust into an exhaust system. The total residence time from the burner to the furnace exit is approximately 2.5 s.

Equivalent Reactor Network

As seen in Fig. 1, the bulk flow patterns are delineated in the regions assigned by APP from the CFD simulation. The baseline PR flame consists of a core, mixing layer, ERZ (which is inconsequential), OFA-region and burnout (BO) region. All other flames have the same regions. The CSTR network from the APP analysis of the baseline PR flame also appears in Fig. 1. The networks for all other CRF flames have similar branches and feedstreams but appreciably different quantitative specifications. In the network, the flame core has been subdivided into two regions. The devolatilization zone covers the upstream portion of the core in which volatiles are being released from the fuel suspension and burned with primary air. Since the primary stream is extremely reducing, no residual O_2 leaves the devolatilization zone. The NO_X reduction zone covers the downstream portion of the core in which only the N-species are converted under the influence of water gas shifting, due to the absence of O_2. The CSTR-series for the mixing layer and the OFA zone represent the mixing of secondary and tertiary air streams, respectively. But there are no additional flows into the CSTR-series for the BO zone.

The RTD for this particular core was deconvoluted into one component for 16 CSTRs-in-series and another for plug flow with respective mean residence times of 138 and 193 ms. The plug flow component represents the near-axial fluid motion under the influence of particle drag, and the CSTR-component represents flow with significant radial velocities. The networks for other fuels usually have only one flow channel for the entire core, and the bulk flow pattern is plug flow. The RTD for the mixing layer was matched with a series of 19 CSTRs, and that for the OFA zone was represented by 6 CSTRs-in-series. The BO zone is essentially in plug flow.

Note that entrainment into the various CSTR-series is represented as a series of discrete additions over several reactors in the series. Volatiles are entrained into the series for the first part of the flame core; secondary air is entrained into the series mixing layer; and tertiary air is entrained into the series for the OFA zone. The addition rates of volatiles were specified from the stand-alone devolatilization simulation with the thermal histories of particles from the CFD simulation. The specific addition rates of the air streams were specified from the continuous entrainment profiles evaluated from the CFD simulation.

Reaction Mechanisms

The devolatilization submodel, called FLASHCHAIN®, determines the complete distribution of volatile

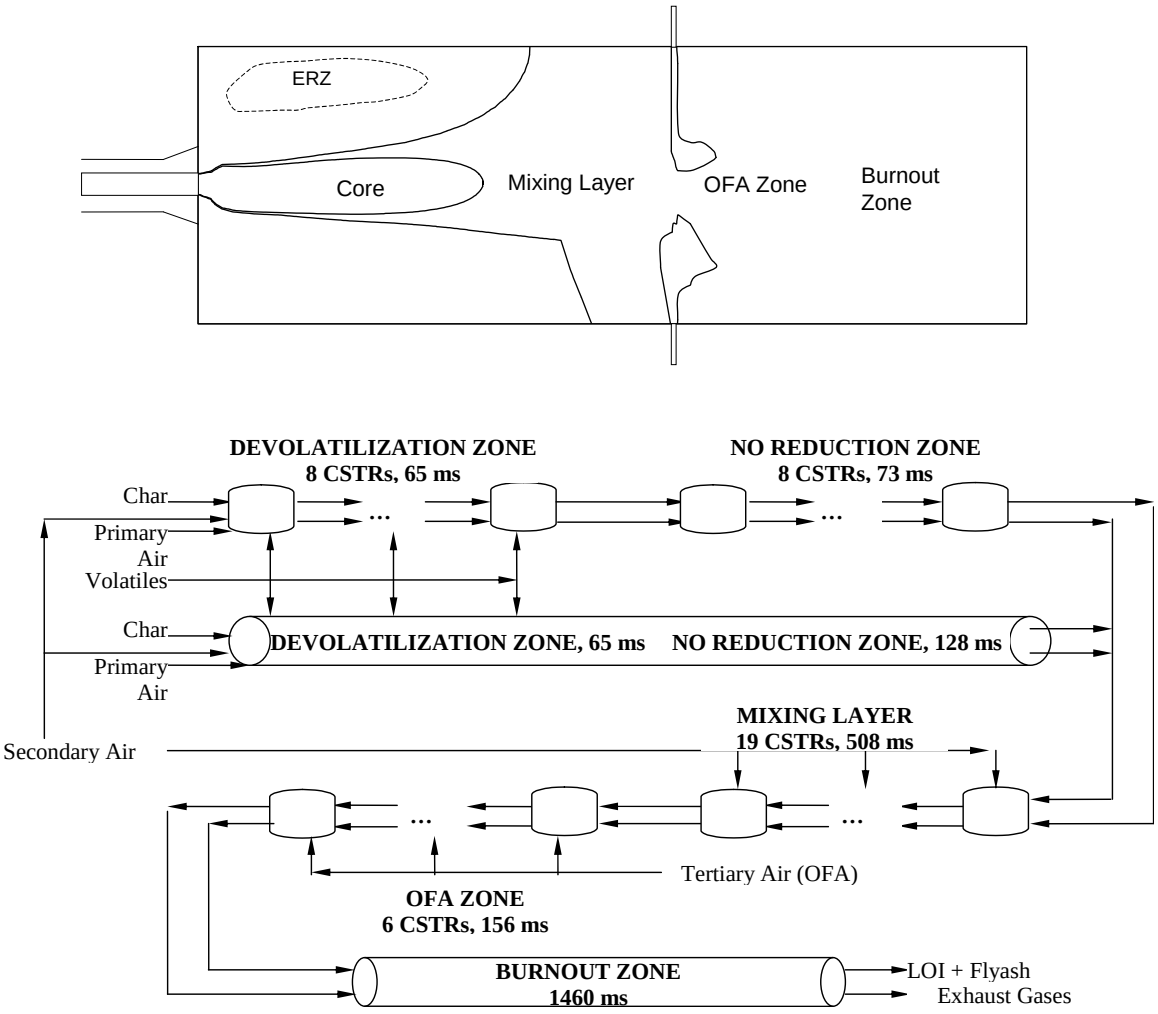

Figure 1. (Top) APP regions delineated from the CFD simulation for the baseline PR flame, and (Bottom) equivalent reactor network.

compounds from almost any p. f., and also predicts the yield and elemental composition of char (Niksa 1995). When combined with a swelling factor correlation and a correlation for the initial carbon density in char, it specifies all the necessary char properties for a char oxidation simulation. Hence, the complete distribution of volatiles, including gaseous fuels and soot, and all char properties are completely determined from only the fuel's proximate and ultimate analyses.

The reaction mechanism for chemistry in the gas phase contains 444 elementary reactions among 66 species, including all relevant radicals and N-species (Glarborg et al. 1998). All rate parameters were assigned independently, so there are also no adjustable parameters in the submodel for gas phase chemistry. The soot chemistry submodel depicts several important effects. As soot burns, it directly competes for the available O_2 and also consumes O-atoms and OH that would otherwise sustain homogeneous chemistry. Soot also promotes recombinations of H-atoms and OH that could also sustain homogeneous chemistry (Pedersen et al. 1999). And soot reduces NO directly into N_2.

Char burning rates are determined by thermal annealing, ash encapsulation (of low-rank chars), and a transition to chemical kinetic control. The Char Burnout Kinetics (CBK) Model includes all these effects, and depicts the impact of variation in gas temperature, O_2 level, and char particle size within useful quantitative tolerances (Hurt et al. 1997). However, it is not yet possible to specify the initial char reactivity within useful tolerances from the standard coal properties. We must calibrate this value with LOI predictions or some other suitable index on combustion efficiency. The submodel for char-N conversion is subject to a similar calibration requirement (with NO emissions), compounded by its simplistic mechanistic premise; viz., that a fixed fraction of char-N is converted into NO at the overall burning rate throughout all stages of char oxidation.

To summarize, the initial char reactivity and the fraction of char-N converted to NO can only be specified from calibration procedures, whereby these parameters are adjusted to match the predicted LOI and NO_X emissions to reported values for a single set of operating conditions. Then the same values should be imposed for all other operating conditions. Except for these two parameters, all other model parameters can be assigned from the fuel's proximate and ultimate analyses within useful quantitative tolerances, or directly adopted from literature.

Calibration and Extrapolation Procedures

The fraction of char-N converted to NO during char oxidation was assigned to fit the NO_X emissions from the coal-only baseline flames for each coal sample. These same values were applied in all cofiring simulations. Values for biomass were unnecessary because biomass chars contain no nitrogen.

Only 13 CFD simulations were developed for the CRF under this project, yet almost 300 tests were simulated with detailed reaction mechanisms. All but one of the cases with CFD simulations had 15 % OFA, and were for the coal-only baselines or the high loading of biomass. Extrapolations to operating conditions without CFD were based on perturbations to the flame temperature profiles and air entrainment rates. All these procedures were established for the coal-only baseline flames to describe the reported impact of furnace stoichiometry and staging level on the NO_X emissions. Once established, the same extrapolation procedures were then applied without adjustment to the cofiring cases.

RESULTS

The discussion in this section moves through the mechanistic basis for NO_X reduction via biomass cofiring, beginning with the distinctive devolatilization behavior of the various fuels in the testing program. Then the NO_X predictions are evaluated in comparisons with data, followed by our interpretations for the major trends based on the detailed flame structure of CRF flames.

Predicted Devolatilization Behavior

Since the heating rate of primary air in the CRF is very fast, the primary devolatilization products are instantaneously converted into secondary volatiles pyrolysis products. The predominant transformation during secondary pyrolysis is the conversion of tar into soot, with simultaneous release of tar-O as CO, tar-H as H_2, and most of the tar-N as HCN. In addition, all aliphatic hydrocarbons are converted into CH_4 and C_2H_2, which can add to the soot phase during the latest stages. The predicted distributions of secondary pyrolysis products are collected in Table 2. Total volatiles yields are the same for both forms of biomass and, at 86 daf wt. %, much higher than the yields from any of the coals. The biomass product distributions are dominated by CO, with substantial amounts of hydrocarbons, especially CH_4, and CO_2 and H_2O. H_2 is another major fuel compound from biomass. But there is surprisingly little soot, considering that tar, the soot precursor, is 25 to 45 % of the daf fuel mass released during primary

Table 2. Distributions of Secondary Pyrolysis Products and Char Properties.

	SD	SG	JR	GL	PR	JW
Volatiles, daf wt. %						
Wt. Loss	86.1	86.0	65.2	56.5	59.8	39.7
Soot	4.3	13.4	30.1	33.7	37.9	26.8
CH_4	7.1	7.4	0.7	0.4	0.5	0.3
C_2H_2	2.2	1.3	1.5	1.0	1.3	2.3
C_2H_4	1.4	1.5	0.0	0.0	0.0	0.0
H_2	2.1	1.7	3.4	3.6	4.0	3.5
CO	48.4	41.5	12.9	7.2	6.1	1.7
CO_2	8.2	8.0	6.4	2.2	1.7	1.0
H_2O	12.1	7.7	7.6	4.9	4.3	1.8
HCN	0.0	0.0	1.26	2.47	2.24	1.52
NH_3	0.24	2.90	0.0	0.0	0.0	0.0
H_2S	0.0	0.44	0.42	1.17	1.91	0.96
Char Comp., daf wt. %						
C	94.7	97.1	98.9	98.4	98.5	98.2
H	3.4	2.5	0.5	0.5	0.4	0.5
O	1.9	0.4	0.0	0.0	0.0	0.0
N	0.0	0.0	0.4	1.1	1.0	1.26
S	0.0	0.0	0.1	0.1	0.1	0.0
Char ash, wt. %	2.5	75.7	15.9	14.2	30.9	21.8
Char size, μm	97.6	103.6	29.9	59.1	54.1	41.7

devolatilization. The reason is the abundance of tar-O, which approaches 40 % of the tar mass. This oxygen converts most of the tar into CO rather than soot during secondary pyrolysis. Essentially all the fuel-N is released as NH_3 during secondary pyrolysis. The abundance of NH_3 with switchgrass, and its higher soot yield and lower CO yield, are the major difference between the two biomass forms.

In contrast, the secondary pyrolysis products from all the coals are dominated by soot which is, by far, the most abundant product. The total hydrocarbon yields are comparable from all coals, but less than a fourth of the hydrocarbon yields from the biomass. Hydrogen yields are also comparable, and double those from biomass. The yields of the oxygenated gases diminish with coals of progressively higher rank, in accord with the trend in the coal-O levels. But even the highest CO yield from JR coal is only about one-quarter the CO yield from the biomass. The only N-species is HCN although, in actuality, a minor amount of NH_3 may have been released from JR coal (but none of the others). The N-species yields are directly proportional to the coal-N levels, as expected.

Char compositions are very similar among all six fuels, except that the most abundant heteroatoms in biomass chars are H and O versus H and N in the coal-derived chars. The char-N levels are negligible in biomass chars. They are comparable but lower for the coal-derived chars and certainly not negligible. Perhaps the most significant variation in char properties is among the char-ash levels. The values for SG and PR are definitely high enough to inhibit char oxidation during the latest stages of burnout, according to the ash inhibition mechanism in CBK. The mean char sizes are disparate for the biomass and coal chars, but more similar than the whole coal values because biomass shrinks and the coals swell during devolatilization, especially the bituminous coals.

Evaluation of Predicted NO_X Emissions

The reported impact of fuel quality on NO_X emissions is extremely complex. It depends on which coal is fired, which biomass is cofired, which cofiring level is imposed, and which injection configuration is used. Table 3 presents the measured and predicted NO_X emissions for all cases with co-milled fuel injection and 15 % OFA that had 3.5 % exhaust O_2. Cofiring with 10 % sawdust always reduced NO_X, except with JR coal (and with GL coal with 0 % OFA). With the same injection, cofiring with 20 % sawdust reduced NO_X with JR and GL but not with JW. With PR/20 % SD, NO_X was reduced with 15 % OFA (but not with 0 % OFA). Cofiring with 20 % SG was effective on PR and JW, but not with GL and JR. With 10 % SG, cofiring was effective with JR, but not with GL and JW; PR was not tested at this condition.

As seen in Table 3, the predicted emissions for PR hv bit coal (Ser. 1) are within experimental uncertainty for all biomass cofiring combinations. They correctly depict the more-than-20 % reduction in NO_X with the highest loadings of both biomass forms, and a proportional decrease in NO_X for progressively higher biomass loadings. No discrepancy exceeds 16 ppm. Similarly, the predictions for JR subbit. (Ser. 7) depict the proportional reductions in NO_X with higher biomass loadings, and the greater effectiveness of sawdust compared to switchgrass. In this series no discrepancy exceeds 35 ppm. Cases with the JW lv bit. coal are within experimental uncertainty for switchgrass co-firing (Ser. 13), which did not reduce NO_X at either of the lower switchgrass loadings. The predicted NO_X reduction with 20 % switchgrass (Ser. 12) was under 10 %, in accord with the measured value. But with sawdust cofiring on JW coal (Ser. 12), the predictions show no significant NO_X reduction for any sawdust loading, at odds with the reported reductions up to 11 % for loadings of 10 and 20 %.

Predicted NO_X emissions with GL coal (Ser. 5 and 6) are not as accurate as all others, and the reported behavior is more complex. With sawdust cofiring, the reported extent of NO_X reduction is significantly greater for a 10 % loading than for 20 %. With switchgrass cofiring, the same extent of NO_X reduction was reported for both loadings. But the predicted NO_X emissions are actually higher than the coal-only baselines with both biomass forms. Unfortunately, no CFD simulations were available for any of the GL test cases, so the specifications for PR-coal were applied in all GL-cases. A breakdown in this extrapolation procedure may be responsible for the discrepancies in the predictions, although they may also reflect a flaw in the mechanisms for this particular chemical environment.

The accuracy of the extrapolation procedures for furnace stoichiometry and staging level are apparent in Fig. 2. This set of predictions covers the full ranges of furnace stoichiometry (which determines exhaust O_2 level) and degree of air staging in the test program. The predictions are based on the procedures developed to fit the NO_X emissions for the coal-only baseline tests over the same domain of conditions, starting with only a single CFD simulation for 3.5 % O_2 and 15 % OFA. The same procedures were then applied without modification to the biomass cofiring cases, such as the 15 % SG on PR in Fig. 2. The predictions are within experimental uncertainty except, perhaps, for the highest O_2 level with 15 % OFA. Notwithstanding, it is evident that these extrapolations did not introduce intolerable uncertainties into the predictions, and APP can be successfully applied with many fewer CFD simulations than test conditions.

DISCUSSION

The predicted structure of the flame core for the PR/20%SD flame appears in Fig. 3. In contrast to SG, SD has almost no fuel-N. This cofired flame still generates 25% less NO_X than the PR-only baseline flame, which is slightly more than the reduction expected for the removal of fuel-N alone. The time scale in Fig. 3 depicts the core as well as the first quarter of the mixing layer. For this particular test, devolatilization is completed within 80 ms, and the flow leaves the core at 118 ms. The total residence time in the mixing layer is 476 ms, but only the first 150 ms are shown in Fig. 3. The S. R. value for the

Table 3. Evaluation of Predicted NO_X for 3.5 % O_2 with 15 % OFA.

Series	Fuel	NO_X, ppm @ 3 % dry O_2	
		Pred.	**Mes'd**
1	PR hv bit	325	328
	PR/10%SD	255	271
	PR/20%SD	236	245
	PR/15%SG	277	269
	PR/20%SG	258	260
5	GL hv bit	372	360
	GL/10%SD	365	273
	GL/20%SD	318	327
6	GL hv bit	368	356
	GL/10%SG	399	340
	GL/20%SG	349	336
7	JR subbit	263	240
	JR/10%SG	203	185
	JR/20%SG	177	142
	JR/10%SD	221	191
	JR/20%SD	212	189
12	JW lv bit	419	422
	JW/5%SD	416	420
	JW/10%SD	417	389
	JW/20%SD	436	364
13	JW lv bit	429	450
	JW/5%SG	422	455
	JW/10%SG	442	440
	JW/20%SG	404	407

gas phase falls sharply while volatiles are released into the flow, making it more reducing. It then relaxes to an ultimate value 0.864, which is significantly more reducing than both the PR-only baseline and the PR/20%SG flame. Although SD and SG have identical volatiles yields, the gas phase in the SD-core becomes more reducing because more CO and less soot are produced by the primary volatiles from SD.

Initially, the CO concentration surges during the ignition period, then increases more gradually during the oxidation of char and soot. Its ultimate value and the persistence of H_2 reflect water gas shifting once all O_2 has been consumed. The maximum CO concentration is double that in the PR/20%SG flame. The H_2 mass fraction persists at roughly 1000-2000 ppmw across the entire core. Moreover, hydrocarbons, especially C_2H_2 (not shown), persist at 1000 ppmw or more across the entire devolatilization zone. This is the only flame core with an appreciable amount of hydrocarbons in the presence of NO, although their concentration is still much lower than those of CO and H_2.

As for the other flames, almost half the char burns out in the core, but hardly any soot burns out in this particular core. The more reducing character of the gas phase in this core imparts several distinctive features to the N-species conversion chemistry. The N-speciation is dominated by HCN and NO, as for the PR-only baseline flame. The NH_3 released by the SD is rapidly converted to HCN and NO within 40 ms. But NO does not accumulate at the expense of HCN, as in both of the other flame cores. Instead, the HCN concentration surges while NO accumulates. Some prompt N-fixation mechanisms involving N_2 in air must be responsible because the total maximum amount of fixed-N species is double the maximum

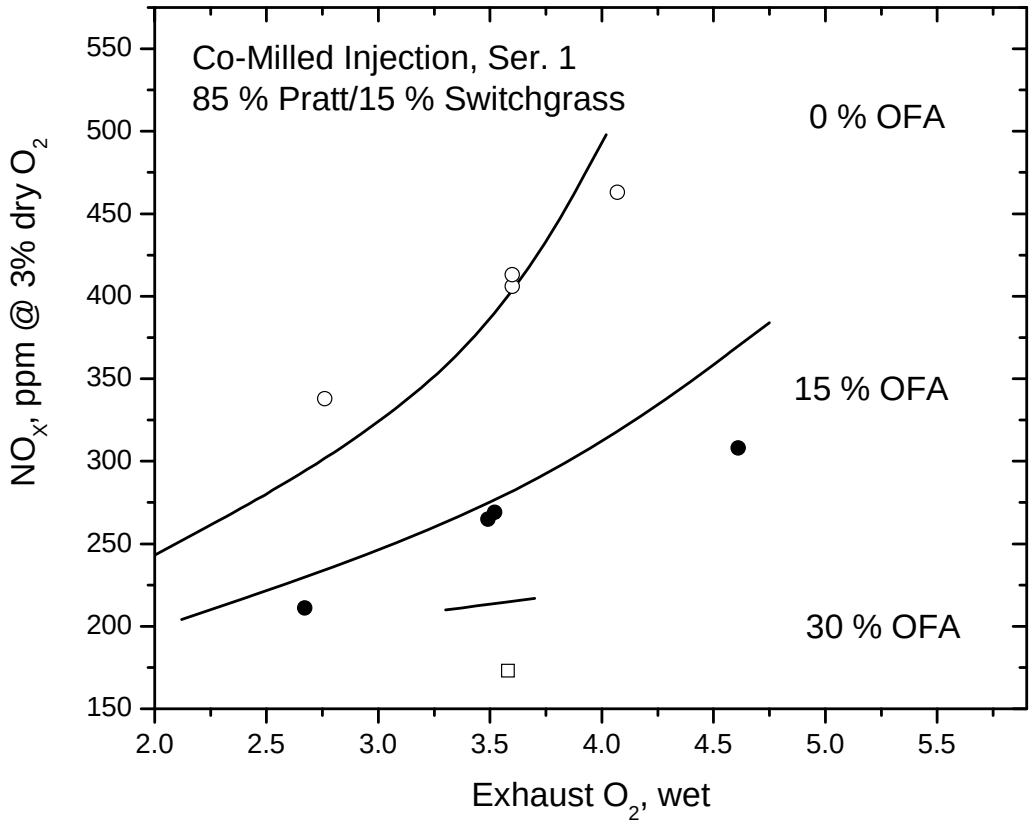

Figure 2. Predicted (Curves) and measured (data points) NO_X emissions for 3 staging levels and a range of exhaust O_2 levels for PR/15 % SG flames.

value in the PR/20%SG flame, and the SG-cofired flame has significantly more volatile-N. NO reduction begins at 75 ms but by the exit of the core, there is still 1390 ppmw HCN and 465 ppmw NO, which are both much higher than in either of the other flames. Early in the mixing layer, NO reduction accelerates while the HCN concentration plummets. The NH_3 concentration reaches 92 ppm before vanishing with the HCN concentration. The ultimate NO concentration after both other fixed-N species have been eliminated is only 143 ppmw, which is 25 ppm lower than the analogous level in the PR/20%SG flame. Even though there was a higher concentration of fixed-N species in the core, the greater reducing potential yielded a lower NO concentration in the mixing layer, after chemistry in the gas phase was exhausted. Since the extents of char burnout at this point are comparable for the PR/20%SG and PR/20%SD flames, the 20 ppmw reduction for the PR/20%SD flame persists in the exhaust emissions.

A surge in the extent of soot burnout coincides with the entrainment of secondary air. Due to the high maximum temperatures in the mixing layer, the extent of soot oxidation eventually overtakes the extent of char oxidation at 220 ms. The soot burns out in the mixing layer, whereas char is carried over into the OFA and BO regions.

The structures of the coal-only and the biomass cofired flames in the CRF are qualitatively similar: All exhibit a very rapid surge in the NO level immediately after injection, due to the ignition of volatiles under the very lean conditions associated with the primary streams during the initial stages of

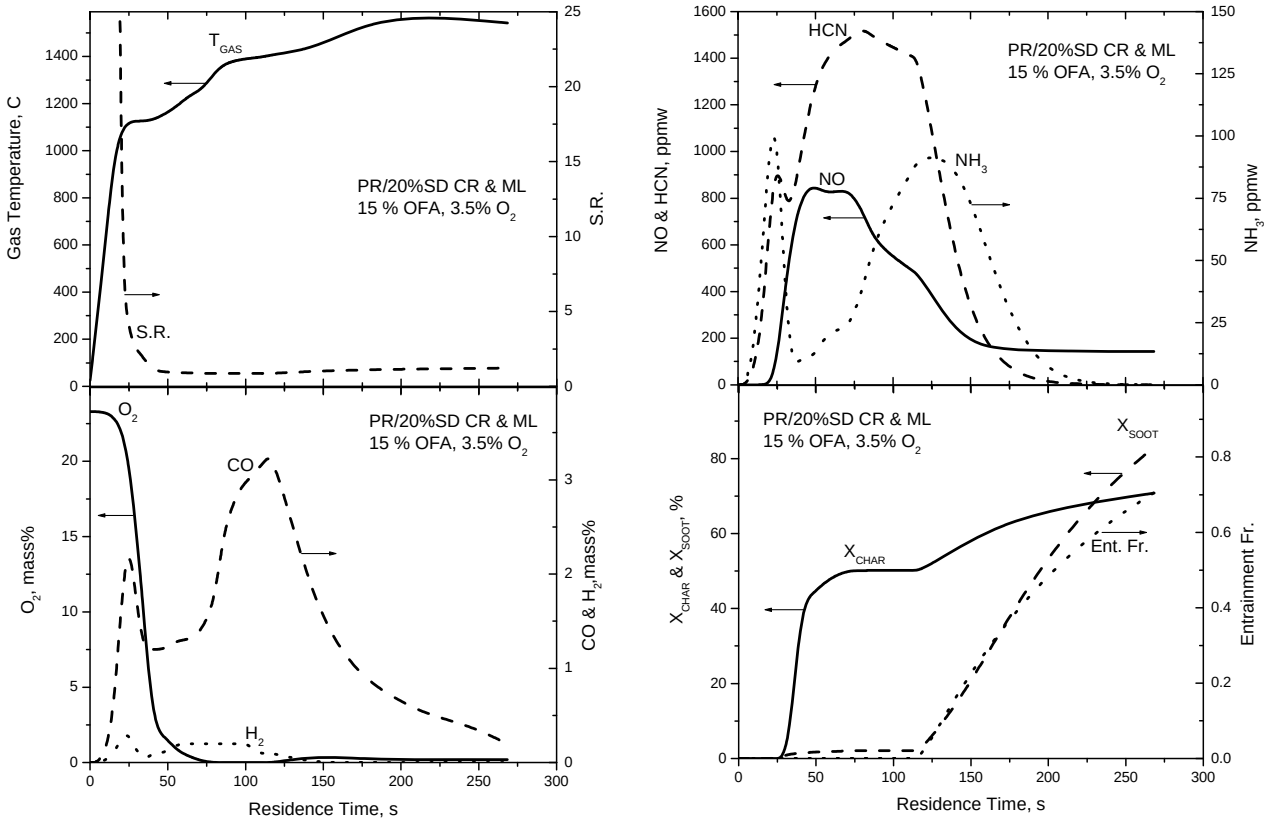

Figure 3. Structure of the core of the PR/20%SD flame showing, in counterclockwise order from the upper left, the operating conditions, major species, char and soot burnout, and N-species.

devolatilization. But as more volatiles are released, the gas phase becomes progressively more reducing, which enables the early NO to be reduced into HCN and NH_3. The extent of reduction is determined by the S. R. value among the gaseous species only and the residence time available before the core fluid is exposed to secondary air in the mixing layer. All fixed-N species are rapidly converted into NO and N_2 at the beginning of the mixing layer, which then sustains the oxidation of soot and char. From this point onward, chemistry in the gas phase is inconsequential, and the conversion of some of the char-N into NO supplements the NO_X inventory.

Two factors are primarily responsible for the significant NO_X reduction observed for CRF flames with biomass cofiring. First, there is more volatile matter from biomass and it contains a much smaller contribution from soot. Consequently, the near-burner S. R. values for the gas phase are significantly richer than in coal-only flames. Under richer conditions, near-burner NO will be reduced away and a greater proportion of the fixed-N species will be converted into N_2. CRF flames provide sufficient residence times in the flame cores for NO reduction and fixed-N conversion to N_2. Second, a significantly lower percentage of the total fuel-N will remain in the char beyond the near-burner zone, where its partial conversion to NO is inevitable. If the biomass contains nitrogen, it releases all of it in the near-burner zone. If the biomass contains no nitrogen, then the inventory of char-N beyond the flame core is reduced in proportion to the biomass loading. In either case, there is less char-N beyond the point where NO can be reduced by chemistry in the gas phase.

The first factor is especially sensitive to fuel quality. Indeed, even the NO_X emissions from the four coal-only flames are ordered according to the volatiles yields and contributions from soot. While the volatiles yields decrease and the soot contributions increase for coals JR, PR, GL, and JW (cf. Table 2), the baseline NO_X emissions in the staged flames increased from 240 to 338 to 358 to 436 ppm (cf. Table 3). Biomass cofiring mitigated these differences by enhancing volatiles yields and by reducing the soot contributions. The net effect was significant NO_X reduction for the cofired flames, even when the biomass supplements the inventory of fuel-N. The extent of reduction was directly proportional to the biomass loading with both forms of biomass on JR and PR coals. But it was only proportional to the switchgrass loading in flames cofired with JW coal; cofiring JW with sawdust was ineffective at all but the highest loadings. Cofiring GL coal reduced NO_X, but the magnitude was disproportionate at 10 % loadings with both biomass forms.

ACKNOWLEDGEMENT

This work was sponsored by an award (DE-FC26-00NT40895) under the Biomass Cofiring Opportunities Program administered by the National Energy Technology Laboratory.

REFERENCES

Glarborg, P., Alzueta, M. U., Dam-Johansen, K., Miller, J. A., Combust. Flame. 115:1-27 (1998).

Hurt, R. H., J.-K. Sun, and M. Lunden, Combust. Flame 113(1/2):181 (1997).

Monroe, L. S. et al., 1995, EPRI/EPA 1995 Joint Symp. On Stationary Combustion NO_X Control, Book 3, EPRI, Palo Alto, CA.

Niksa, S. and G.-S. Liu, "Advanced CFD Post-Processing for P. F. Flame Structure and Emissions," 28th Int. Technical Conf. on Coal Utilization and Fuel Systems, Coal Technology Assoc., Clearwater, Fl, March, 2003.

Niksa, S. and G.-S. Liu, Fuel, 81(18):2371-85 (2002a).

Niksa, S. and G.-S. Liu, Proc. Comb. Inst. 29, to appear (2002b).

Niksa, S., Combust. Flame. 100: 384-394 (1995).

Pedersen, L. S., Glarborg, P., et al. Combust. Sci. and Technol. 132: 251-314 (1998).